National Institute of Standards and Technology • U.S. Department of Commerce

Report of Test

Absolute Spectral Radiance Responsivity

of the

NASA GLAMR Si Radiometer
Model LTD-11, S/N 104

Request Submitted by:

Joel McCorkle
NASA Goddard Space Flight Center
Greenbelt, MD

1. Description of Calibration Items

The device under test (DUT) consists of a silicon radiance meter manufactured by L-1 Standards and Technology, Inc. (L-1), model LTD-11, S/N 104 (referred to as GLAMR Si) along with accessory components consisting of a temperature controller and transimpedance amplifier. The device is housed in a 2-inch diameter tube with fore-optics consisting of two apertures to form a Gershun-tube radiometer. The detector is temperature controlled (L-1 model 3100-1L, S/N 12105) at 29.0 °C and the rear of the device has inputs for the L-1 temperature controller and a BNC output for the detector signal. The detector came with an L-1 model 3300v2, S/N 027, transimpedance amplifier which was used for the calibration. Figure 1.1 shows the detector and accessory equipment as received packaged with the indium gallium arsenide (IGA) and extended-indium gallium arsenide (ex-IGA) radiometers and accessory components.

Figure 1.1 Photographs of GLAMR Si Radiometer as received consisting of the L-1 temperature controller (left), transimpedance amplifier (middle), and radiometer (right). The temperature controller and transimpedance amplifier were received together with the same components for the IGA and exIGA radiometers whereas the Si radiometer was packaged with the IGA radiometer.

1.1 Calibration Request

The request was to calibrate the DUT, GLAMR Si, for absolute radiance responsivity from 320 nm to 400 nm with a standard uncertainty of 0.28 % (k=1) or better and from 400 nm to 885 nm with a standard uncertainty of 0.06 % (k=1) or better.

2. Description of Test

The DUT was characterized for absolute spectral radiance responsivity on the NIST facility for Spectral Irradiance and Radiance responsivity Calibrations using Uniform Sources (SIRCUS).[1,2] The calibration took place in various stages from May 26, 2021 to June 24, 2021. During each calibration test, the detector was temperature controlled at 29.0 °C by the L-1 controller and checked at the beginning and end of each calibration session. This calibration was performed in two parts. First, the spectral range 380 nm to 950 nm was performed using T-06 as the standard reference detector. Second, the spectral range 310 nm to 420 nm was performed using an ultraviolet (UV) enhanced detector, IRD WS #2, as the standard reference detector. Corrections to the radiance responsivity of the DUT were also made to account for sphere fluorescence contributions to the source spectrum at wavelengths between 300 nm to 400 nm. Measurements of the sphere fluorescence were conducted during October and November 2021 to determine correction factors which were later applied to the original calibration data.

Description of laser systems used: Several laser systems were used to cover the specified ranges for the various parts of the calibration.

1. A Picosecond mode-locked lithium triborate-optical parametric oscillator (LBO-OPO) laser (~80 mHz repetition rate) was used that consists of two separate cavities. The main cavity is designed to oscillate the signal beam and the other cavity is designed to intracavity double the oscillated idler beam.
   a. The signal output of the main cavity was used between 775 nm and 950 nm.
   b. The signal output from the main cavity was doubled in a beta-barium borate (BBO) crystal (second harmonic generation, SHG) and used from 380 nm to 526 nm.
   c. The output of the intracavity doubled laser was used from 540 nm to 600 nm.
2. A 4-(Dicyanomethylene)-2-methyl-6-(4-dimethylaminostyryl)-4*H*-pyran (DCM) dye laser (CW, Coherent CR699) was used from 608 nm to 690 nm.
3. A VERDI V-10 laser (solid state diode pumped neodymium-doped yttrium orthovanadate, Nd:YVO_4, frequency doubled) was used for a single point at 532 nm.
4. A femtosecond (~ 100 fs pulse width) mode-locked Ti:Sapphire laser (Spectra Physics Mai Tai) was used in three ranges.
   a. The Mai Tai output was used from 692 nm to 780 nm.
   b. Second Harmonic Generation of the Mai Tai output was used from 380 nm to 400 nm when T-06 was the reference detector and from 350 nm to 400 nm when IRDWS#2 was the reference detector.
   c. Third Harmonic Generation of the Mai Tai output was used from 320 nm to 340 nm when IRDWS#2 was the reference detector.

The laser output was coupled to an optical fiber. The optical fiber was in turn connected to a side port on the integrating sphere and illuminated an area toward the front of the sphere. For the DCM dye laser and VERDI V-10 laser, a section of fiber was placed into an ultrasonic bath to reduce effects due to laser speckle. For the LBO-OPO and Mai Tai systems, the ultrasonic bath was not

required where speckle effects are inherently reduced by laser bandwidth. For each laser, a Brockton Electro-Optics Corporation (BEOC) laser power controller (LPC) stabilized the beam to less than the 0.1 % level using feedback from a photodiode in the sphere, removing short term as well as long term fluctuations in the power output from the various laser sources. A Coherent WaveMaster (S/N: W0385) measured the wavelength for the DCM dye laser and VERDI V-10. For the Mai Tai system, a portion of the beam was directed to an integrating sphere and the wavelength was measured with an Ocean Optics, Inc. JAZ spectrometer (S/N: JAZA0657) that has been calibrated to a mercury pen lamp. For the SHG and THG of the Mai Tai system, the wavelength was measured by a CAS spectrometer (#710314215) whose wavelength scale was calibrated by pen lamps and peak wavelength determined by a spectral fitting analysis. For the LBO-OPO system, a Bristol 621 wavemeter (S/N: 6208) was used to measure the vacuum wavelength of the signal beam. In the case of the externally doubled LBO-OPO, the signal vacuum wavelength was measured directly, and the actual wavelength value was determined as $\lambda = (\lambda_{measured})/2$. For the intracavity doubled LBO-OPO, the signal wavelength was measured directly, and the actual wavelength was determined according to equation 2.1,

$$\lambda = \frac{1}{2\left(\frac{1}{\lambda_{pump}} - \frac{1}{\lambda_{signal}}\right)} \tag{2.1}$$

where λ_{pump} is 532.2 nm in vacuum, λ_{signal} is measured by the Bristol wavemeter in vacuum, and the factor of two converts to the second harmonic of the idler. All wavelengths measured by the Bristol wavemeter were the vacuum value and then converted to the air value for data analysis by dividing by a factor of 1.00027 after completing wavelength conversions. All other wavelengths were measured in air.

Integrating Sphere: The integrating sphere used for radiance responsivity was a LabSphere 30.48 cm (12-inch) diameter, Spectralon-coated sphere equipped with a 5.08 cm (2-inch) diameter exit aperture fabricated by LabSphere (non-point source geometry).

Data Acquisition and Control Program: The data was acquired using a modified version of the SIRCUS Main Program LabVIEW program. The modified version (SIRCUS Program MERLIN 2020.vi) allowed use of an instrument that communicates via GPIB . It was otherwise identical to the typical LabVIEW program and has no effect on the data collection for GLAMR Si. This program was used so that the calibration could be completed simultaneously with another radiometer that required GPIB interface. Background subtracted DC signals were sequentially collected for each detector (DUT and reference standard) along with simultaneously recorded monitor signals (also background subtracted). The collections were repeated 11 times. Each repeat sample was ratioed to the monitor signal and the average and percent standard deviation were determined.

Description of calibration detectors: The working standard reference trap detector T-06 was used to measure the radiance and irradiance emitted from the source sphere from 380 nm to 950 nm. It was equipped with an aperture having an area of 19.6591 mm^2 and a precision transimpedance amplifier, femto SIRCUS 12, was used with the trap detector. T-06 was previously calibrated for power responsivity directly against the NIST Primary Optical Watt Radiometer (POWR).[3–5] The irradiance responsivity scale for T-06 is derived from the power responsivity scale and the area of the precision aperture, which was determined by the NIST aperture area

measurement facility.[6]

The standard reference detector for the UV range was IRD WS #2 and was used to determine the radiance of the source from 320 nm to 420 nm. IRD WS #2 was previously calibrated for power responsivity directly against POWR from 300 nm to 400 nm.[7] The irradiance responsivity was determined from the power responsivity and the aperture area, which was previously determined radiometrically to be 9.660 mm^2 from an irradiance responsivity calibration against a trap detector (T-01) in the range 400 nm to 450 nm. The irradiance responsivity of IRD WS #2 above 400 nm comes from the SIRCUS calibration against T-01 from 400 nm to 450 nm.[8] The transimpedance amplifier used with this detector was SIRCUS Prec. #2.

The monitor detector was a silicon photodiode mounted directly to the source sphere. It was connected to a Stanford Research Systems current preamplifier (Model SR570, S/N: 57687).

3-axis stage: The integrating sphere is mounted on an XYZ translation stage, with the Z-position (along the optical axis) measured with a linear encoder. The X- and Y-axes enable the source to be properly positioned in front of an instrument before it measures the sphere radiance. The Z-position is used to accurately determine the separation between relevant apertures.

Measurement Setup: Detectors used in these experiments were mounted to tip-tilt stages and aligned to the optical axis of the integrating sphere source using a double-headed laser. To align the detectors to the sphere, the double-headed laser was first mounted in-front of the large sphere where one end of the laser was previously aligned to the center of the sphere aperture. The other end of the laser was retroreflected from a glass microscope slide on each detector to align to the optical axis. Lastly, the laser was centered on each detector using the 3-axis stage to determine the X,Y position. See Figures 2.1 and 2.2 for photographs of the measurement setup and Figure 2.3 for a photograph of the temperature controller and transimpedance amplifier setup.

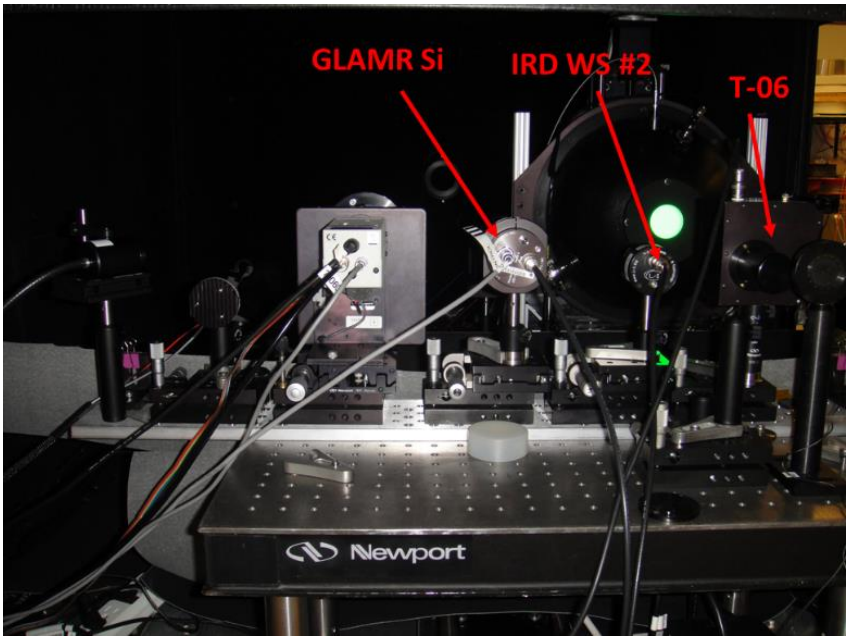

Figure 2.1 Back-view of detector bench setup for the radiance measurements of the DUT using both T-01 and IRD WS #2 as the standard reference detectors.

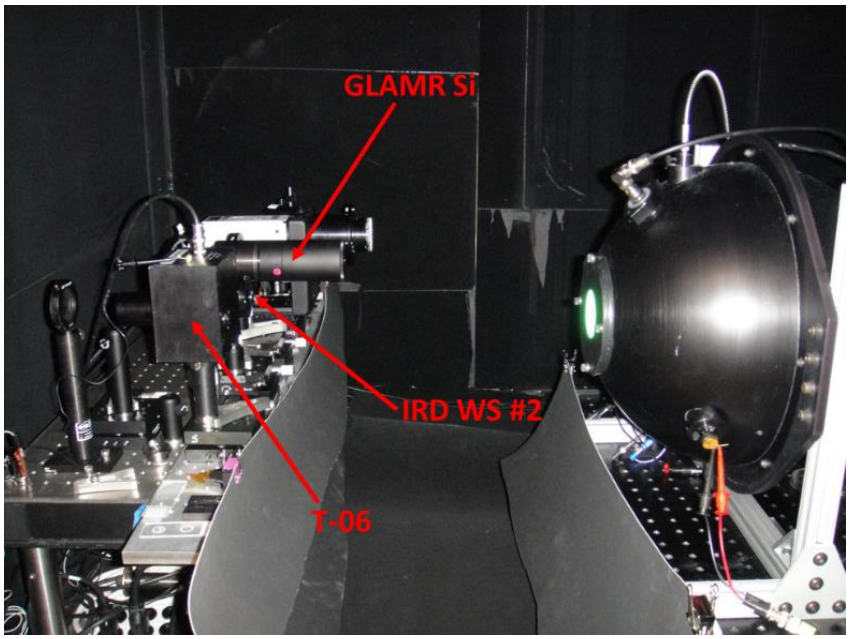

Figure 2.2 Side-view of detector bench setup for radiance measurements of the DUT using both T-01 and IRD WS #2 as the standard reference detectors.

Figure 2.3 Photograph showing the setup of the GLAMR temperature controllers and transimpedance amplifiers

Description of sphere fluorescence measurements: For source wavelengths ranging from 300 nm to 400 nm, the sphere source output spectrum was measured using a CAS spectrometer (CAS 710314215) equipped with an irradiance head (E-head). The spectrometer used the factory

default linearity correction and was calibrated for wavelength by pen lamps. To isolate the sphere fluorescence contributions to the source output spectrum, the CAS E-head was illuminated by the sphere and directly illuminated by the source optical fiber placed in a separate holder. The CAS E-head was aligned to the sphere or optical fiber holder in typical fashion utilizing the XY stage in the SIRCUS box. Flux levels were controlled during each spectral acquisition using the LPC such that the same collection parameters could be used for both the sphere and fiber data collections.

2.1 Radiance Responsivity of GLAMR Si from T-06 and IRD WS #2

Absolute radiance responsivity measurements for GLAMR Si (with associated transimpedance amplifier) versus the UV protected reference standard detector, IRD WS #2, and trap detector, T-06, were completed at discrete wavelengths between 310 nm to 420 nm and 380 nm to 950 nm, respectively, using the SIRCUS facility. The integrating sphere source was the 12" diameter sphere described in Section 2 with a 5.08 cm (2") aperture and was placed at a fixed position relative to both GLAMR Si and the reference detectors at position Z = -431.7 mm. This placed the sphere approximately 28 cm from the GLAMR Si aperture and placed the field of view completely withing the 2-inch diameter sphere output aperture. An X-Y response map was also measured for the DUT, verifying the central position and underfilled configuration of the DUT relative to the sphere aperture. For the reference detectors, the sphere position placed it well within the acceptance angle of the working reference detector for power measurement as suggested in Section 3.1, below. The working distance was determined for both reference detectors from the sphere Z-position and the radiometrically determined detector position, as described in Section 3.2 below.

The pre-amplifier gain setting for GLAMR Si was generally 1 x 10^6 V/A for all measurements. For T-06, most measurements were done with gain setting 1 x 10^6 V/A. A gain correction factor is known for the T-06 preamplifier (Femto SIRCUS 12) for 1 x 10^7 V/A gain setting of 1.0012. At a gain setting 1 x 10^6 V/A a gain correction factor of 1.0028 was determined by taking a measurement at each gain setting. For IRD WS #2, the gain setting was 1 x 10^7 V/A for THG wavelengths 320 nm to 340 nm and was otherwise 1 x 10^6 V/A. There was no gain correction factor for IRD WS #2 associated with the known high accuracy gain settings for the SIRCUS Prec #2 amplifier.

3. Results of Test

For this calibration, a radiance calibration measurement was performed using two different reference detectors depending on the wavelength range of interest. The reference detector (trap T-06 or IRD WS #2) measures the radiance emitted from the source sphere. Even though the reference detectors are irradiance meters, they are also used to determine the source radiance, requiring knowledge of the solid angle of the source at the detector aperture. To determine the solid angle, the distance between the reference detector aperture and the integrating sphere source aperture was measured, along with the integrating sphere and trap aperture areas: See Section 3.1. The reference detector positions are determined radiometrically, as described in Section 3.2, and the distance of each from the source was determined by measuring the Z-position with the linear encoder on the Z-axis stage. Separate measurements were also completed to determine fluorescence contributions to the sphere radiance at wavelengths between 300 nm to 400 nm. Corrections were made to the DUT radiance responsivity in this wavelength range as described in Section 3.3.

3.1 Determination of the sphere source radiance when using irradiance meters

The radiance of the sphere source was determined with the flux transfer method. A working reference detector (T-06 or IRD WS #2) measured the radiant power from the sphere source passing through two precision apertures, one on the source side, another on the detector side.

The radiance L [W m^{-2} sr^{-1}] of the sphere was determined from radiant power P [W] and the geometric extent G by:

$$L = \frac{P}{G} \tag{3.1}$$

The geometric extent G [m^2 sr] is given by

$$G = \frac{\pi^2}{2}\left[(d^2 + r_s^2 + r_D^2) - \{(d^2 + r_s^2 + r_D^2)^2 - 4r_s^2 r_D^2\}^{1/2}\right] \tag{3.2}$$

where r_S is the radius of the aperture in front of the source, r_D is the radius of the aperture in front of the detector, and d is the distance between the two apertures. The diameter of the sphere aperture was large enough (50.8 mm) to overfill the radiance measurement angle of the DUT radiometer by the sphere output radiation. The distance, d, was chosen large enough (383.25 mm for T-06 and 389.87 mm for IRD WS #2) so that the sphere aperture was well within the acceptance angle of the working reference detector for power measurement.

3.2 Detector offset and offset uncertainty determination for irradiance meters

For radiance measurements of the sphere source using an irradiance meter, knowledge of a distance between the source and the reference detector aperture is required. This distance was determined radiometrically. At several different Z positions, the detector and monitor voltages were recorded to yield a relative irradiance. Using the $1/Z^2$ law for on-axis irradiance (inverse square law) the resultant data can be fit by a point-source geometry (Equation 3.3) and a non-point-source geometry (the experimental configuration, Equation 3.4) to yield the Z-position of the detector aperture plane. From the Z-position encoder reading used in the radiance and irradiance measurements and the detector Z-position from the radiometric $1/Z^2$ law fit, the actual detector aperture to sphere aperture distance in millimeters (working distance) was determined. Figure 3.1 is a schematic of the configuration.

The inverse square law fitting equation for a point-source geometry is:

$$y = \frac{m_1}{(M_0 - m_2)^2} \tag{3.3}$$

Where y is the relative irradiance, m_1 is a fitting constant, M_0 is Z-position of the integrating sphere that is read by the Z-encoder, and m_2 is the Z-position of zero offset between the two apertures. The fitting uncertainty in m_2, for the sphere position during calibration, gives the uncertainty in the distance between the two apertures.

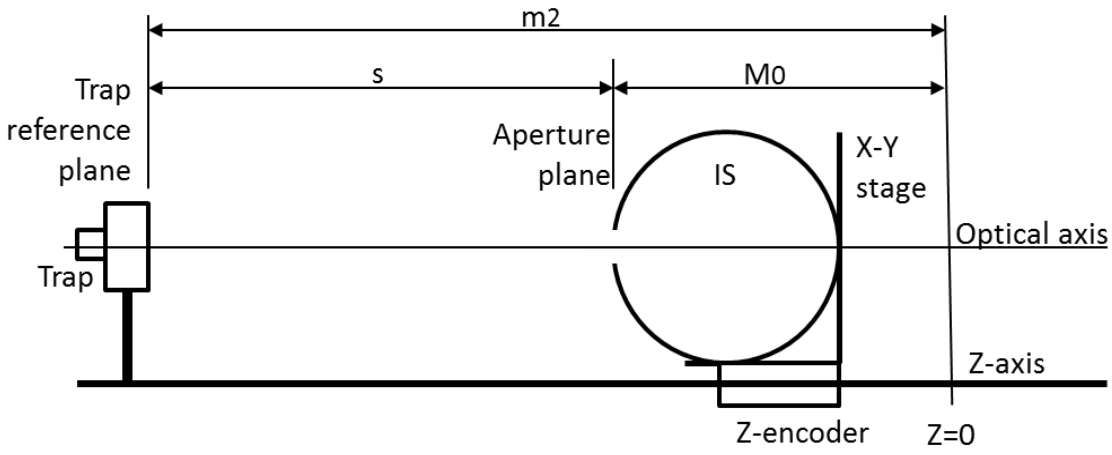

Figure 3.1. Schematic of the configuration for determining trap-sphere distance radiometrically.

If the source aperture is large, the non-point source geometry expression is fit to the data:

$$y = \frac{m_1}{((M_0 - m_2)^2 + m_3^2 + m_4^2)} \tag{3.4}$$

where y, m_1, M_0, and m_2 are the same as in Eq. 3. $m_3 = r_d$, the radius of the detector aperture, and $m_4 = r_s$, the radius of the integrating sphere aperture. Equation 3.4 is valid in the limit where

$$(r_s^2 + r_d^2 + s^2) \gg 2r_s r_d \tag{3.5}$$

and s is the distance between the source and detector apertures. The inverse square law measurements along with the fit of equation 3.4 to the data for each detector can be seen in Figures 3.2 and 3.3, below. At a separation, s, equal to the working distance, the ratio given by equation 3.5 was determined for each detector. This result is summarized in Table 3.1 and shows the condition of equation 3.5 holds and that equation 3.4 is valid in each case. The residuals are approximately 3 orders of magnitude smaller than the base measurement and show there is no obvious bias or offset. The fitting results are also summarized in Table 3.2.

For irradiance responsivity measurements, a correction factor (CF) in the source irradiance arises due to slight differences in the working distance between the DUT and reference standard detectors. The correction factor is determined according to equation 3.6 and the detector radius, r_d, refers to either the standard reference detector or the DUT.

$$CF = \frac{r_s^2 + r_{d,ref}^2 + s_{ref}^2}{r_s^2 + r_{d,ref}^2 + s_{DUT}^2} \tag{3.6}$$

Applying this correction factor gives the source irradiance as measured by the reference standard detector at the DUT reference plane. For radiance responsivity measurements, this correction factor is irrelevant.

Table 3.1 Results of equation 3.5 at minimum separation distances.

Detector	r_s (cm)	r_d (cm)	s (cm)	Ratio (Eq 3.5)
IRD WS #2	2.54	0.175	38.987	1740
T-06	2.54	0.178	38.325	1655

Table 3.2 Results of the inverse square law fits of equation 3.4 to the data.

Detector	m_2 (mm)	Fitting Uncertainty (mm) (k=1)	R, fit
IRD WS #2	-821.57	0.1175	1
T-06	-814.97	0.0611	1

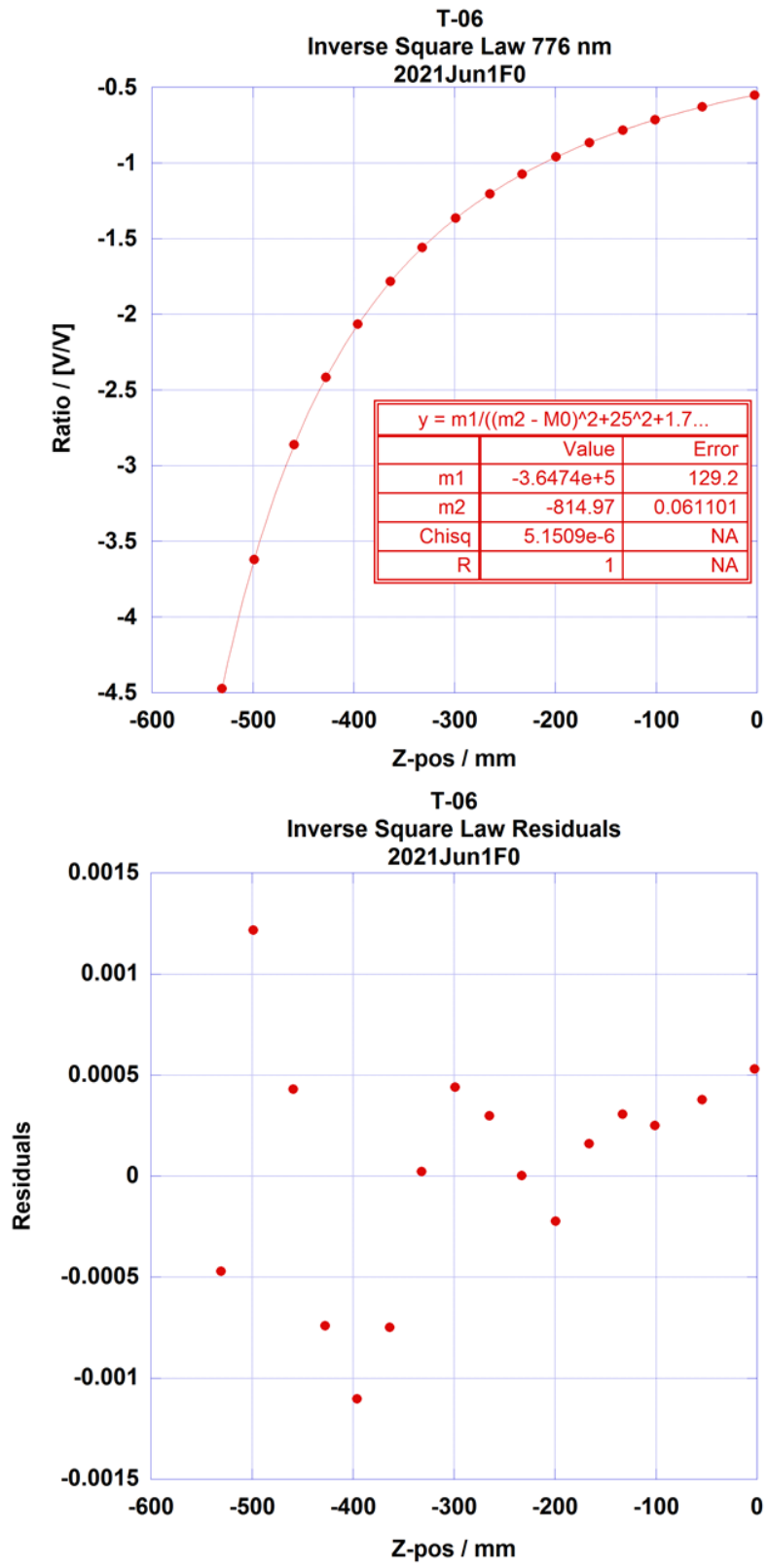

Figure 3.2 Offset and uncertainty fit of the non-point source geometry equation 3.4 to the irradiance response data at a wavelength of 776 nm (top) and residuals from the fit (bottom) for distance determination of T-06.

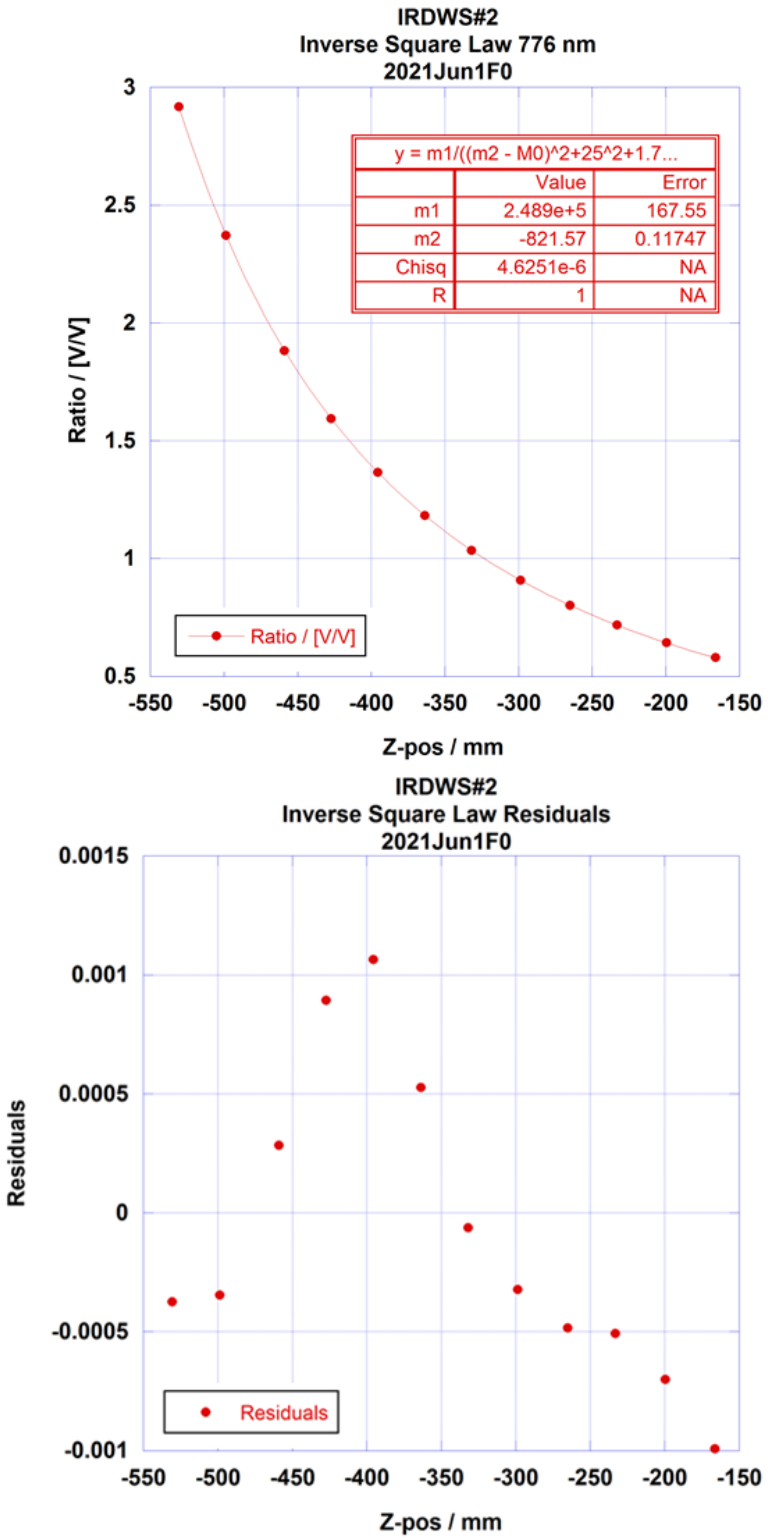

Figure 3.3 Offset and uncertainty fit of the non-point source geometry equation 3.4 to the irradiance response data at a wavelength of 776 nm (top) and residuals from the fit (bottom) for distance determination of IRD WS #2.

3.3 Sphere Fluorescence Measurements and Fluorescence Corrections Factors

At wavelengths between 300 nm to 400 nm, or shorter, the source output is a combination of the narrowband laser light and a broad sphere fluorescence spectrum. Spectra were collected for both the sphere output and bare fiber output to isolate the fluorescence contributions to the overall sphere spectrum. The data were converted to relative radiometric flux units utilizing the relative spectral response function of the CAS (RSR_{CAS}) and then normalized to the peak optical source wavelength. Example spectra collected are shown in Figure 3.4. Spectra from the sphere generally had an excess signal extending out to ≈ 700 nm when compared to the spectra from the fiber and the normalized in-band (IB) regions were quite similar indicating the sphere fluorescence. At a few wavelengths (345 nm to 360 nm) a secondary peak appeared from the fundamental wavelength used in harmonics generation of the UV source light even though a filter was employed. Contributions from the fundamental peak were also included at these wavelengths and lead to a larger correction and higher uncertainty with this effect most significant at 345 nm. There were also small contributions in the spectra due to 2nd order diffraction but the peak at 690 nm in Figure 3.4 (right) was confirmed to be mostly fundamental light by adding an additional filter prior to fiber coupling.

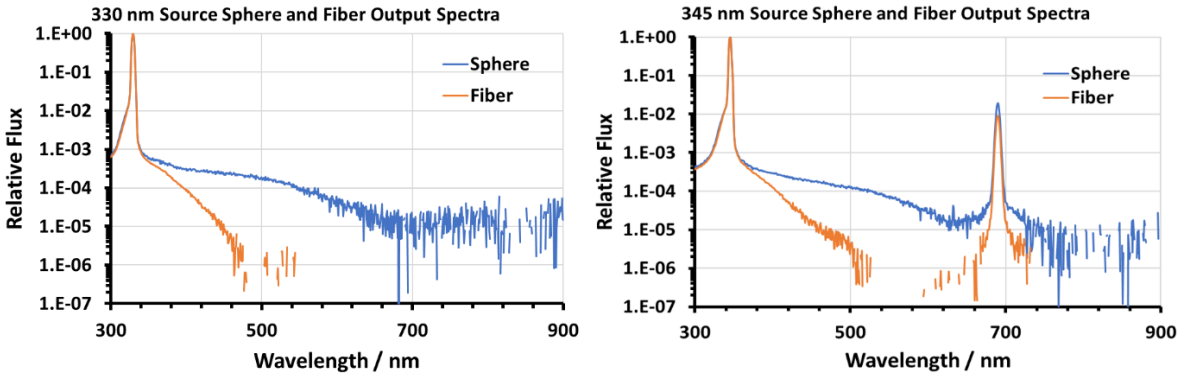

Figure 3.4 Example spectra of the sphere and bare fiber output collected by the CAS at 330 nm (left) and 345 nm (right).

The fraction of fluorescence (or fluorescence plus fundamental) contamination present in the sphere output spectrum was determined by subtracting the integrated out-of-band (OB) portion of the bare fiber spectrum from the integrated OB portion of the sphere output spectrum and dividing by the integrated IB portion of the sphere output spectrum. More importantly, the percent contribution of the OB signal, to the signal measured by each detector in the responsivity calibration (DUT and T-06 or IRDWS#2) was determined utilizing the spectral responsivity of each detector (RESP). The measured spectra are multiplied by the spectral responsivity of each detector and then integrated and subtracted.

Determination of the fractional signal on each detector (f_A, where the subscript indicates either the DUT or reference detector) due to OB contributions to the source spectrum (*i.e.* sphere fluorescence or fundamental source light) as just described is represented by equation 3.7. The CAS spectra of the source emitted by the sphere and bare fiber are E_{sph} and E_{fib}, respectively, the other parameters are already defined, and all parameters are a function of wavelength. The summations are defined over the wavelength range spanning 10 pixels on either side of the peak

for the IB region whereas the OB summation starts from the following pixel and extends several hundred nanometers into the red.

$$f_A = \frac{\sum_{OB} RSR_{CAS} \times RESP_A \times \left(E_{sph} - E_{fib}\right)}{\sum_{IB} RSR_{CAS} \times RESP_A \times E_{sph}} \tag{3.7}$$

For the responsivity calibration, the presence of fluorescence or other contaminants in the OB region of the source spectrum results in extra signal measured by both the DUT and reference detector. In other words, the total signal, S, measured is a sum of the IB and OB contributions or $S = S_{IB} + S_{OB}$. To transfer the calibration from Ref to DUT, the ratio of IB signals S_{IB}^{DUT} and S_{IB}^{Ref} are needed but the total signal, S_{DUT} and S_{ref} was measured. The total signal ratio can be multiplied by a correction factor according to equation 3.8 to obtain the needed IB signal ratio.

$$\frac{S_{IB}^{DUT}}{S_{IB}^{Ref}} = \frac{S^{DUT} - S_{OB}^{DUT}}{S^{Ref} - S_{OB}^{Ref}} = \frac{S^{DUT}}{S^{Ref}} \frac{(1 - f_{DUT})}{(1 - f_{Ref})} \tag{3.8}$$

The correction factor, C_f, is defined by equation 3.9 and is determined from equation 3.7 for each detector.

$$C_f = \frac{(1 - f_A)}{(1 - f_B)} \tag{3.9}$$

In practice, the radiance responsivity of the DUT as determined by the calibration using the contaminated sphere output was simply multiplied by C_f determined later by the sphere fluorescence measurements. The percent signal due to OB contributions on each detector found by equation 3.7 is shown in Figure 3.5 (left) and the corrections factors determined from this data by equation 3.9 for each DUT calibration from the two different reference detectors (T-06 and IRDWS#2) are shown in Figure 3.5 (right). The corrections factors were found at wavelengths not necessarily the same as wavelengths used in the calibration of the DUT, because the sphere fluorescence measurements were done after the initial calibration. For this reason, the corrections factors shown in Figure 3.5 (right) were interpolated to the wavelengths used in the calibration and those values were used to correct the DUT radiance responsivity displayed in Section 3.4, below.

The fluorescence correction factors add an additional uncertainty component to the overall calibration. The uncertainty arises from components due to the uncertainty in the CAS RSR and the detector responsivities ($RESP_A$) used in equation 3.7, and the CAS measurement standard deviation of the mean. These uncertainties were propagated using the NIST uncertainty machine (https://uncertainty.nist.gov/). Another uncertainty component arises by estimating how much the percent fluorescence changes depending on widening the OB integration range. Further into the red regions of the spectrum, the signal is several orders of magnitude reduced from the peak IB signal, so this component represents a small contribution. However, the uncertainty is more

significant when 2nd order diffraction or fundamental source wavelengths appear in the spectrum, as is the case for source wavelengths from 335 nm to 360 nm and most significant at 345 nm. At wavelengths where the fluorescence is most prominent, at shorter wavelengths toward 300 nm, the uncertainties arising from this analysis are highest. The final uncertainties associated with the sphere fluorescence corrections at each wavelength are tabulated in Table 3.3 and included in the total uncertainty budget, below.

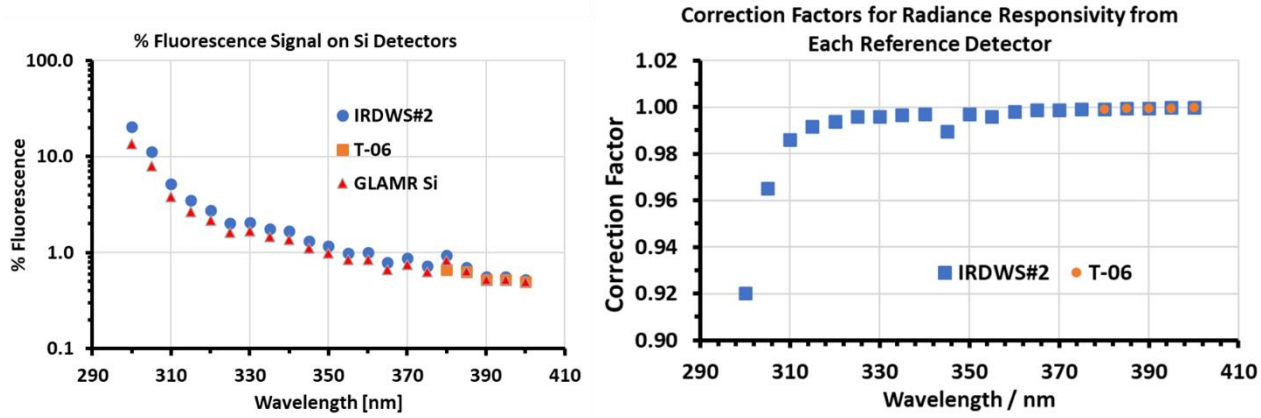

Figure 3.5 Percent fluorescence contributions to the total signal measured by each detector (left) and correction factors (right) determined for the DUT calibration from each reference detector.

Table 3.3: Fluorescence correction factor uncertainty at measured sphere output wavelengths

Wavelength / nm	Uncertainty (%)	Wavelength / nm	Uncertainty (%)
300	2.5	355	0.2
305	0.4	360	0.1
310	0.2	365	0.05
315	0.2	370	0.05
320	0.2	375	0.05
325	0.1	380	0.02
330	0.1	385	0.02
335	0.1	390	0.02
340	0.1	395	0.02
345	0.6	400	0.02
350	0.1		

3.4 Radiance Responsivity of GLAMR Si (LTD-11, S/N: 104)

Radiance responsivity of GLAMR Si was measured from 310 nm to 950 nm using two standard reference detectors to cover the separate but overlapping spectral ranges. Standard reference detector T-06 was used from 380 nm to 950 nm and IRD WS #2 was used from 310 nm to 420 nm as shown in Figure 3.6 for the full range and Figure 3.7 for an expanded view of the UV range. In

the overlap region 380 nm to 420 nm, good agreement within the standard uncertainties was found between the responsivities derived from the two reference detectors. Comparing the absolute values measured when using IRD WS #2 and T-06 at equivalent wavelengths resulted in an average absolute percent difference of 0.09 %. The total data from each reference detector is tabulated in Table 3.4.

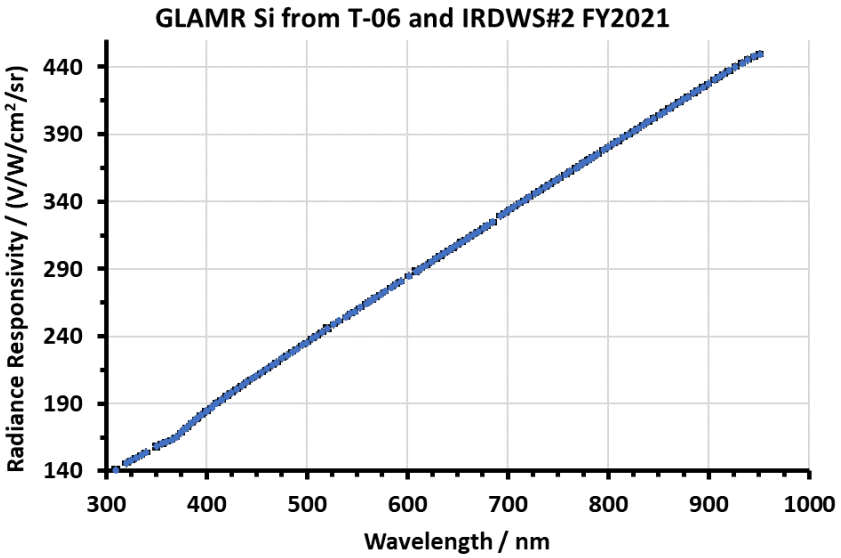

Figure 3.6 Radiance responsivity of GLAMR Si radiometer from T-06 (blue circles) and IRD WS #2 (orange squares). Error bars (black) represent the k=2 absolute uncertainty.

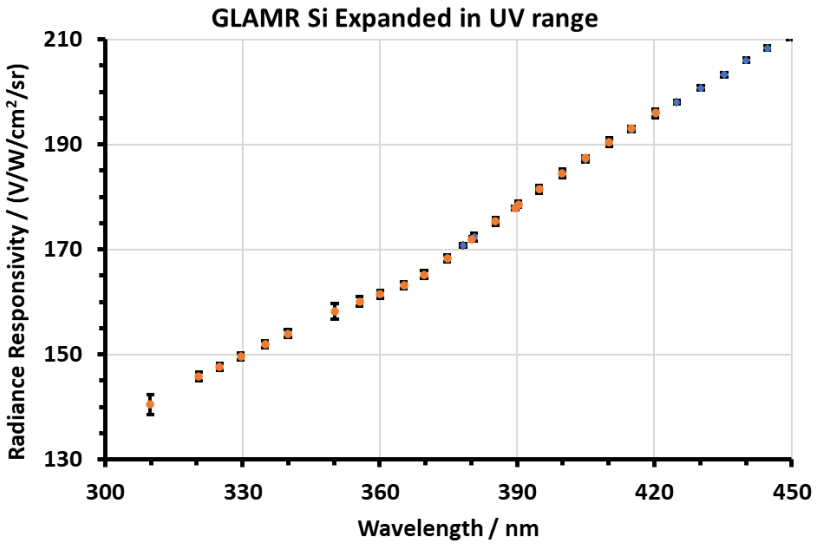

Figure 3.7 An expanded view of Figure 3.4 in the showing the transition region around 400 nm where both T-06 and IRD WS #2 reference detectors were used. Error bars represent the k=2 absolute uncertainty.

Table 3.4 Tabulated absolute spectral radiance responsivity data for GLAMR Si.

Ref Detector	Wavelength [nm]	Radiance Responsivity [V/(W/cm²/sr)]	Total k=1 Uncertainty (%)
IRDWS#2	309.836	140.46	0.68
IRDWS#2	320.467	145.76	0.29
IRDWS#2	324.988	147.70	0.23
IRDWS#2	329.648	149.60	0.23
IRDWS#2	334.938	151.90	0.23
IRDWS#2	339.923	153.97	0.23
IRDWS#2	350.171	158.22	0.48
IRDWS#2	355.563	160.09	0.29
IRDWS#2	360.103	161.48	0.23
IRDWS#2	365.268	163.23	0.21
IRDWS#2	369.694	165.22	0.21
IRDWS#2	374.721	168.33	0.21
T-06	378.195	170.77	0.11
IRDWS#2	380.186	171.99	0.20
T-06	380.599	172.36	0.10
T-06	385.267	175.35	0.10
IRDWS#2	385.267	175.32	0.20
IRDWS#2	389.568	177.91	0.20
T-06	390.263	178.61	0.10
IRDWS#2	390.263	178.57	0.20
T-06	394.795	181.45	0.11
IRDWS#2	394.795	181.44	0.20
T-06	399.872	184.28	0.10
IRDWS#2	399.872	184.54	0.20
T-06	404.908	187.11	0.11
IRDWS#2	404.908	187.40	0.17
T-06	410.087	190.27	0.09
IRDWS#2	410.087	190.41	0.16
T-06	414.970	192.78	0.14
IRDWS#2	414.970	193.04	0.19
T-06	420.191	195.69	0.11
IRDWS#2	420.191	196.00	0.17
T-06	424.871	198.07	0.10
T-06	430.123	200.76	0.11
T-06	435.261	203.28	0.10
T-06	440.042	206.01	0.10
T-06	444.684	208.35	0.10

T-06	449.685	210.42	0.12
T-06	454.792	213.06	0.09
T-06	460.024	215.73	0.09
T-06	465.371	218.39	0.09
T-06	469.750	220.60	0.09
T-06	475.324	223.60	0.10
T-06	480.168	225.95	0.10
T-06	485.410	228.57	0.10
T-06	489.869	230.72	0.10
T-06	495.332	233.45	0.10
T-06	499.944	235.35	0.11
T-06	505.334	238.36	0.11
T-06	509.527	240.46	0.10
T-06	514.777	243.01	0.10
T-06	520.132	245.97	0.37
T-06	526.655	248.82	0.10
T-06	532.090	251.30	0.12
T-06	539.012	254.44	0.13
T-06	543.456	256.73	0.12
T-06	547.463	258.46	0.12
T-06	553.016	261.23	0.10
T-06	559.118	264.46	0.11
T-06	561.446	265.44	0.10
T-06	564.528	266.91	0.10
T-06	568.101	268.66	0.10
T-06	572.984	271.04	0.10
T-06	577.564	273.13	0.10
T-06	584.056	276.36	0.10
T-06	588.672	278.61	0.10
T-06	593.360	280.84	0.10
T-06	601.444	284.82	0.10
T-06	608.250	288.19	0.27
T-06	610.050	288.91	0.18
T-06	613.670	290.51	0.14
T-06	618.620	292.84	0.12
T-06	623.310	295.09	0.12
T-06	628.430	297.68	0.13
T-06	632.520	299.55	0.11
T-06	636.690	301.55	0.11
T-06	641.310	303.81	0.12
T-06	645.320	305.57	0.16
T-06	649.730	307.82	0.14
T-06	653.860	309.95	0.15

T-06	658.010	311.90	0.13
T-06	662.170	313.74	0.14
T-06	666.000	315.71	0.13
T-06	670.540	317.70	0.13
T-06	675.890	320.29	0.14
T-06	679.020	322.04	0.16
T-06	685.070	324.86	0.16
T-06	692.300	329.42	0.10
T-06	697.100	331.71	0.10
T-06	701.900	334.03	0.10
T-06	706.400	336.19	0.10
T-06	711.500	338.62	0.10
T-06	716.600	341.02	0.10
T-06	721.400	343.28	0.10
T-06	726.800	345.86	0.10
T-06	731.600	348.10	0.10
T-06	737.000	350.66	0.10
T-06	741.400	352.73	0.10
T-06	746.800	355.22	0.10
T-06	751.500	357.42	0.10
T-06	757.200	360.15	0.10
T-06	761.900	362.33	0.10
T-06	767.500	364.95	0.10
T-06	771.200	366.70	0.10
T-06	774.992	368.57	0.10
T-06	776.200	369.05	0.10
T-06	779.888	370.87	0.10
T-06	781.900	371.77	0.10
T-06	784.471	373.03	0.10
T-06	789.098	375.28	0.10
T-06	795.357	378.30	0.10
T-06	800.114	380.43	0.10
T-06	805.341	382.97	0.10
T-06	809.409	384.85	0.10
T-06	815.181	387.62	0.10
T-06	820.187	389.92	0.10
T-06	825.255	392.36	0.10
T-06	829.525	394.42	0.10
T-06	834.709	396.93	0.10
T-06	839.954	399.36	0.10
T-06	845.272	401.94	0.10
T-06	850.658	404.43	0.10
T-06	855.200	406.59	0.10

T-06	860.713	409.20	0.10
T-06	865.369	411.39	0.10
T-06	870.528	413.88	0.10
T-06	875.286	416.02	0.10
T-06	879.128	417.80	0.10
T-06	884.961	420.60	0.10
T-06	888.886	422.49	0.10
T-06	894.347	425.11	0.10
T-06	899.371	427.53	0.10
T-06	905.474	430.44	0.10
T-06	910.107	432.53	0.10
T-06	914.785	434.73	0.10
T-06	920.040	437.22	0.10
T-06	926.433	440.10	0.10
T-06	932.919	442.86	0.10
T-06	938.954	445.37	0.10
T-06	945.052	447.61	0.10
T-06	950.664	449.38	0.10

3.4 Uncertainty analysis for the Radiance Responsivity of GLAMR Si (LTD-11, S/N: 104)

	Relative Standard Uncertainty [%]	
Uncertainty Component	**IRD WS #2 310 nm to 420 nm**	**T-06 380 nm to 950 nm**
Reference detector Irrad. Cal.[1]	0.15	0.05
Measurement % St Dev[2]	0.06	0.04
Reference Detector Distance	0.06	0.03
Fluorescence Correction Factor[3]	0.1	0.02
Geometry Alignment	0.05	0.05
Amplifier Gain	0.05	0.05
Reference Detector Aperture Area	0.02	0.02
Sphere Aperture Area	0.03	0.03

Wavelength	0.03	0.03
Total k = 1 % Uncertainty	**0.22**	**0.11**

Note 1: For IRD WS #2 the reference detector calibration uncertainty is 0.12 below 400 nm and 0.17 above 400 nm.
Note 2: This is the average measurement percent standard deviation across the entire range. Values for individual wavelengths can be found in the calibration file.
Note 3: Uncertainty for this component at individual wavelengths between 300 nm and 400 nm are shown in table 3.3. The individual wavelength uncertainty is accounted for in the total uncertainty at each wavelength shown in Table 3.4.
Note 4: This is not the full calibration uncertainty budget. The uncertainty budget, Table 3.4, does not include environmental effects on both the reference detector and the GLAMR radiometer. No evaluations of instrument performance characteristics such as temperature dependence, response linearity or temporal stability were performed. For estimates in the interpolated uncertainty, see the reference.[9]

4. General Information

It should be noted that the reported results for the DUT were obtained using the dial gain value on the provided pre-amplifiers (i.e. 1 x 10^6 V/A). The gain setting is only the nominal value and was not used in the analysis resulting in the reported radiance responsivity units of [V/W/cm^2/sr].

Information was recorded in the SIRCUS Vis #21 laboratory notebook, pp.81-91.

The calibration measurements, data analysis, and report writing were performed by Brian Alberding and John Woodward.

This calibration required 10 days of laboratory work (including setup, troubleshooting, and data collection) on SIRCUS and 7 days of data reduction, analysis, and reporting.

Significant experimental notes:

1. On June 22, 2021, it was noticed the computer had been restarted and the XY stage was powered off, likely due to a power outage on a previous day. After restarting the equipment and rehoming the XY stage data collection continued but analysis of the data revealed a discrepancy compared to data taken prior to the power outage. The discrepancy resulted from homing the stage, where the stage did not home to the same previous position and resulted in the stage being ~ 1 cm low compared to the previously determined alignment positions. The calibration was continued after realigning the sphere.
2. For wavelengths in the UV range below 400 nm, a CAS spectrometer (#710314215) was placed in the SIRCUS enclosure to observe the sphere and check for fluorescence. The CAS spectrometer was calibrated on June 2, 2021, against an FEL lamp (FEL 5194) to yield a *relative* spectral responsivity. This effort was aimed towards evaluating the contribution from fluorescence to the measured irradiance responsivity. The CAS spectrometer was also used to measure the wavelength, where the CAS was calibrated using pen lamps. The peak wavelength was found by a fitting analysis to the spectral response data.

Information about data files:

1. Full data files for the radiance responsivity of GLAMR Si are located on Elwood under:

\\cfs2e.nist.gov\685\internal\G04\SIRCUS\SIRCUS\Calibrations\SIRCUS Calibrations\FY 2021 Calibrations\GLAMR\GLAMR Si

Data file for the radiance responsivity of GLAMR Si: "GLAMR Si Combined Data FY2021_220222.xlsx"

2. Data file for the sphere fluorescence correction is located in the following directory: "Fluorescence Correction_GLAMR.xlsx"

   \\cfs2e.nist.gov\685\internal\G04\SIRCUS\SIRCUS\Calibrations\SIRCUS Calibrations\FY 2021 Calibrations\Sphere Fluorescence

   Data file for the sphere fluorescence correction for GLAMR Si is: "Fluorescence Correction_GLAMR.xlsx"

The files located in these directories are meant for internal NIST use only. Please do not distribute without authorization.

References

1. Brown, S. W., Eppeldauer, G. P. & Lykke, K. R., "Facility for spectral irradiance and radiance responsivity calibrations using uniform sources," *Appl. Opt.*, **45**, 8218–8237 (2006).
2. Woodward, J. T. *et al.*, "Invited Article: Advances in tunable laser-based radiometric calibration applications at the National Institute of Standards and Technology, USA," *Review of Scientific Instruments* **89**, 091301 (2018).
3. Houston, J. M. & Rice, J. P., "NIST reference cryogenic radiometer designed for versatile performance," *Metrologia* **43**, S31–S35 (2006).
4. Shaw, P.-S., "Report of Calibration for SIRCUS Si Trap Detectors T06 and T04 from 475 nm to 1000 nm," (2016).
5. Shaw, P.-S., "Report of Calibration for SIRCUS Trap Detectors T06 and T04 from 364 nm to 470 nm," (2017).
6. Fowler, J. & Litorja, M., "Geometric area measurements of circular apertures for radiometry at NIST," *Metrologia* **40**, S9–S12 (2003).
7. Shaw, P.-S., "Report of Calibration: Spectral Power Responsivity based on Absolute Cryogenic Radiometer for Si photodiodes SN IRD WS #1, IRD WS #2, UVG #16, and UVG #24," (2017).
8. Alberding, B. G. & Woodward, J. T., "Report of Test: Absolute Spectral Radiance Responsivity of the NASA GLAMR Si Radiometer Model LTD-11, S/N: 104," 685.04/SRS2019-002(2019).
9. Gardner, J. L., "Uncertainties in Interpolated Spectral Data," *J. Res. Natl. Inst. Stand. Technol.* **108**, 69–78 (2003).

Distribution Restrictions: None

Tabulated calibration data files were provided along with this report.
Filename: "GLAMR Si Combined Data FY2021.xlsx"

Prepared by:

BRIAN ALBERDING
Digitally signed by BRIAN ALBERDING
Date: 2022.03.30 16:29:13 -04'00'

Brian G. Alberding
Remote Sensing Group
Sensor Science Division
Physical Measurement Laboratory
(301) 975-4664

Approved by:

JOSEPH RICE
Digitally signed by JOSEPH RICE
Date: 2022.03.30 17:13:23 -04'00'

Joseph P. Rice, Leader
Remote Sensing Group
Sensor Science Division
Physical Measurement Laboratory
(301) 975-2133